A STUDY ON NUMERICAL COUPLING BETWEEN MECHANICAL AND HYDRAULIC BEHAVIORS IN A GRANITE ROCK MASS SUBJECT TO HIGH-PRESSURE INJECTION

Woo-Chang Jeong[1], Dominique Bruel[2], and Jai-Woo Song[3]

[1] Research Center for Disaster Prevention and Safety Management, Hong-Ik University, Seoul, Korea
[2] Centre d'Informatique Géologique, Ecole Nationale Supérieure des Mines de Paris, France
[3] Department of Civil Engineering, Hong-Ik University, Seoul, Korea

Abstract: An injection experiment was carried out to investigate the pressure domain within which hydromechanical coupling influences considerably the hydrologic behavior of a granite rock mass. The resulting database is used for testing a numerical model dedicated to the analysis of such hydromechanical interactions. These measurements were performed in an open hole section, isolated from shallower zones by a packer set at a depth of 275 m and extending down to 840m. They consisted in a series of flow meter injection tests, at increasing injection rates. Field results showed that conductive fractures form a dynamic and interdependent network, that individual fracture zones could not be adequately modeled as independent systems, that new fluid intakes zones appeared when pore pressure exceeded the minimum principal stress magnitude in that well, and that pore pressures much larger than this minimum stress could be further supported by the circulated fractures. These characteristics give rise to the question of the influence of the morphology of the natural fracture network in a rock mass under anisotropic stress conditions on the effects of hydromechanical couplings.

Key Words: hydromechanical interactions, fracture zone, high-pressure injection, stress, granite rock mass

1. INTRODUCTION

Characterizing and modeling the hydromechanical behavior of a natural fractured rock mass still remains a challenging problem in various engineering fields such as civil engineering, petroleum engineering and engineering geology. Multiple disciplines that were often used independently are now being integrated and we may expect significant improvements of our understanding. Flow through single fractures of varying apertures is generally investigated (see the review by Zimmerman and Bodvarsson, 1996) as a function of aperture distribution parameters and contact area. The effect of normal stress to explain the deviation from the well-known cubic law at large stress levels, at the sample scale or at larger scale as reported by Raven and Gale (1985) is also widely discussed. Numerous empirical models have been proposed

for the normal closure behavior of joints (Bandis et al., 1983; Brown and Scholz, 1985). The relationships between the fracture stiffness, as a link between the hydraulic and seismic properties of a single natural fracture, are also reported (Pyrak-Nolte, 1992). Unger and Mase (1993) propose a theoretical model where the aperture distribution is determined during the closure of two random elastic surfaces. During closure, asperities that come into contact deform elastically and deformations are transmitted through the infinite half-space to neighboring asperities. Capasso et al.(1999) use a similar approach using an elasto-plastic behavior for the contact zones. Both approaches lead to a non-linear dependency between normal stress, ratio of contact area and mean closure. They provide at each stress levels the parameters required by Zimmerman and Bodvarsson (1996) formalism to derive the equivalent hydraulic conductivity of a rough fracture.

An application at the field scale of coupled models using such nonlinear stress-closure relationships is illustrated by Rutqvist (1995) on single fractures isolated in vertical boreholes by two impermeable packers. The purpose is to determine their normal stiffness from well tests, namely pulse tests and hydraulic jacking tests. However the tensile situation cannot properly be reproduced in these simulations without starting to adjust additional parameters, like the fracture size, the fluid pressure at the fracture tip or the Young's modulus of the surrounding rock blocks. Coupling between flow along a given fracture and stresses across this fracture under site specific conditions is therefore dependent upon the global mechanical behavior of the host rock and the hydraulic conditions at the fracture boundaries or at intersections with other fractures, that will control the overall fluid pressure field.

Modeling of the rock mass as an assemblage of discrete blocks separated by joints, using a distinct element method, as in the UDEC package (Cundall and Hart, 1985), is then very suitable. In this approach, blocks may be rigid or deformable. They interact and transmit loads from fractures to fractures. Developments involving fluid flow and thermally induced stresses and displacements (see for instance, Abdallah et al., 1995) are proposed to address a wide range of physical situations. Finite element methods also provide attractive capabilities for the analysis of such couplings in fractured and fractured-porous rocks. A detailed review is given in Stephansson et al. (1996).

The present contribution reports on a field study where the rock mass may not be accurately represented by a persistent system of blocks and joints. They are run in a granite settlement, in order to determine the pore pressure level for which the hydromechanical coupling must be taken into account (Cornet and Morin, 1997). Pressures larger than the minimum effective normal stress are observed in a borehole during injection tests. These findings, which corroborate previous results obtained in 1987 during several weeks long pumping tests at this same site (Bruel and Cornet 1995), are discussed with the help of a numerical model.

2. DESCRIPTION OF THE NUMERICAL MODEL

This section describes the basic principles and capabilities of a numerical model dedicated to the coupling of rock deformation and flow through fractures in hard rocks. Some details referring to the geometry that can be handled and to the treatment of the hydraulic and mechanical interactions are given hereafter.

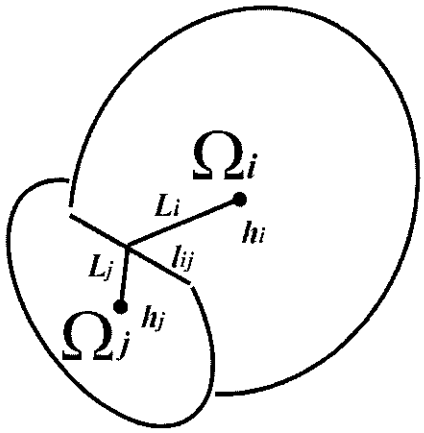

Fig. 1. Ω_i and Ω_j are the centers of two connected elements. L_{ij} is the length of their intersection. L_i is the distance between Ω_i and the mid-point of the intersection segment. h_i is the hydraulic head at center of Ω_i

2.1 Geometric specificities: numerical mesh of a multiple fracture system

In the proposed discrete approach, the basic geometrical object is a disc, as illustrated in Fig. 1. The fractures are arrangements in space of arrays of discs. Fractures are planar, with a finite extension, and elliptical in shape. They are fixed in space throughout the numerical simulations and cannot propagate. Parameters used to describe such a crack are two sets of three coordinates (focus point of the ellipse) and the half-length of the principal axis. Each fracture is meshed into a number of adjacent cells, of constant size, (a square lattice aligned with the principal axis of the ellipse). The whole set of cells is then merged into the volume of rock to be modeled. Cells that fall out of this volume are discarded. Those that crosscut this limit (top, bottom, vertical boundary, inner boundary) are assigned particular codes for further numerical treatments. An implicit assumption of the present approach is that cells at the edge of a fracture will act as closed boundary for flow. Fluid enters the network at particular cells (e.g. where a borehole crosscut the fractures), and moves along the fractures that may intersect each other. Leakage occurs at cells connected to the boundaries. The typical scale of an elementary cell is 1-10 meters, and all the parameters are taken constant within such an element (ratio of contact area, aperture, pressure, normal stress, shear stress, change in aperture, temperature etc.).

2.2 Mechanical model

Rock mass is infinitely large, homogeneous, isotropic and linearly elastic. The fractures are considered to be two-dimensional discontinuity where small relative displacement between both surfaces may occur, when the shear stress exceeds the shear strength as given by the Mohr-Coulomb failure criterion. Tensile condition leads to the opening of the corresponding element. The displacements are constant within each element of the network.

Consider a right-handed Cartesian local coordinate system $(\Omega_i, u_1^i, u_2^i, u_3^i)$, such that the plane (i.e. $u_3^i=0$) represents the ith element of the fractured network, centered at point Ω_i. Let φ_1^i, φ_2^i and φ_3^i represent the components of a displacement discontinuity φ^i affecting the ith element. Following sign conventions that are used, a compressive stress is positive and a negative value of φ_3^i indicates the ith element being opened.

According to the previous assumptions, the displacement discontinuity technique presented by Crouch (1976), allows to express the change of the stress at any point j in the rock mass as a linear function of the displacement discontinui-

ties φ^i affecting all the fracture elements. The resulting induced traction vector t^j, which components are $\Delta s_{13}^j, \Delta s_{13}^j$ and Δs_{33}^j can be expressed as

$$\{t^j\} = \sum_i [A^{ji}]\{\varphi^i\} \tag{1}$$

where $[A^{ji}]$ is an influence matrix (3×3) which describes the effect of displacements of joint i on the stress at joint number j. The influence coefficients $[A_{kl}^{ji}]$ in Eq. (1) are functions of joint location, joint orientation and material properties of the intact rock (i.e. Young's modulus E and Poisson's ratio ν). For square elements, these coefficients are given in an extensive form through analytical development by Sinha (1979).

Depending on boundary conditions given at each of the n elements, a set of n equations is set up and can be used to obtain the corresponding $3 \times$n unknown displacements that produce these prescribed conditions. These boundary conditions are commonly expressed in terms of normal and shear stresses with respect to local coordinates. They take into account the regional stress field s_0 and the water pressure field ψ. Three different models are proposed :

2.2.1 Closed fracture

This case is that both upper and lower surfaces of a fracture are in contact, and applies when total normal stress $[t_{03}^i + t_3^i - \psi_i]$ is high enough to prevent the fracture to be sheared. In this case, induced normal and shear stresses across the element are governed by its own shear and elastic moduli, i.e. a 3×3 diagonal stiffness matrix $[K^i]$.

$$\{t^i\} = [K^i]\{\varphi^i\} \tag{2}$$

Since the deformation acts upon the joint material, the corresponding displacements are generally small, so that the induced stress effects on the surrounding elements can be neglected. Considering the global influence matrix, it is desirable to turn a closed element into a rigid element, and therefore Eq. (2) reduces to

$$\{\varphi^i\} = \{0\} \tag{3}$$

The resulting compressive normal stress is stored for the hydraulic purpose.

2.2.2 Open fracture

In this case, both upper and lower surfaces of a fracture (with respect to the local coordinates) are separated. Fluid pressure applies in the normal direction and the supported shear is reduced to zero. This leads to the following equation for a given element i :

$$\{t_o^i\} + \{t^i\} = \{p^i\} \tag{4}$$

where $t_0^i = s_o \cdot u_3^i$ is the local stress vector supported by the ith element and p^i is a prescribed fluid pressure vector which components are $(0, 0, \psi_i)$.

2.2.3 Sheared fracture

Each fracture represents a surface of weakness in the rock mass, such that changing in fracture fluid pressure and rock stress can cause the fracture to become unstable, resulting in shear slip along the fracture surfaces and an associated change in fracture hydraulic aperture. The total shear stress vector across a fracture element i are constraint by a linear Mohr-Coulomb relationship. When the resultant

shear stress given as $\tau_i = \sqrt{(t_{01}^i + t_1^i)^2 + (t_{02}^i + t_1^i)^2}$ is higher than the limiting value $\tau_i^{\max}$ equal to

$$\tau_i^{\max} = \tan(\Phi)(t_{03}^i + t_3^i - \Psi_i) + S \tag{5}$$

where Φ and S are the internal friction angle and the cohesion respectively, slip occurs and corrections are applied to the φ_1^i and φ_2^i components, to minimize this difference $\tau_i - \tau_i^{\max}$ toward zero. The φ_3^i component is set to zero and the resulting compressive normal stress is stored.

2.3 Hydraulic model

We assume that the flow is entirely restricted to the fracture network and that the fluid does not enter into the matrix. A hydraulic conductivity value has to be assigned to each cell in the fracture network. These are drawn from a modified cubic law, which applies for one-dimensional laminar flow between two parallel plates. Per unit distance in the fracture width direction, this hydraulic conductivity is given by

$$k = f \times k_0 \tag{6}$$

where k_0 is a reference value defined at each fracture element under zero effective stress conditions, as follows:

$$k_0 = \frac{\rho g e_0^3}{12\mu} \tag{7}$$

where, ρ [kgm^{-3}], μ [kgm^{-1}s^{-1}] and g [ms^{-2}] are fluid density, viscosity and acceleration of gravity respectively.

The aperture e_0[m] is a model parameter, that can vary from cell to cell according to a distribution function, and that has to be calibrated. The coefficient f can be lower or greater than unity, depending on the following discussion.

2.3.1 Closed fracture

In the case of a mechanically closed fracture, the normal effective stress is positive and there are some areas in contact in between the opposite faces of the fracture cells that delineate voids and potential tortuous paths for the fluid. The morphology of the connections between the neighbouring voids controls the whole fracture permeability. This point was reviewed by Zimmerman and Bodvarsson (1996) and it comes out that reasonably accurate predictions of the hydraulic conductivity can be made using the first two moments μ_e and σ_e of the aperture distribution and the proportion of contact area c = 1- a, a being the void's ratio per unit area, according to the following expression for the pre-factor f:

$$f = \left(1 - 1.5\frac{\sigma_e^2}{\mu_e^2}\right)(1 - 2c) \tag{8}$$

For varying confined situations, corresponding to different effective stress levels, it is known from experiments (Gentier, 1986) performed at the sample size, that the voids ratio varies nonlinearly with the normal loading. Therefore the coefficient a, and both moments μ_e and σ_e have to be continuously defined as a function of the effective stress. Quantitative approaches are available to build these relationships (Unger and Mase, 1993; Capasso et al., 1999). The present model considers an empiric exponential relationship between a and the normal stress σ_n and the pressure ψ. In the absence of reliable knowledge at depth for the aperture field description, it is also assume that Zimmerman's formulation for the pre-factor f can be

replaced by the combination of two empiric laws, respectively describing the voids ratio evolution with normal stress, and f as a function of this voids ratio. Jeong (2000) shows how these empiric functions can be built and evaluated against pre-existing formulations. Flow along rough single fractures is extensively simulated using geostatistical and fractal descriptions for the initial aperture distribution.

$$a = a_0 + (1 - a_0)\exp\left[-\frac{(\sigma_n - \psi)}{p}\right] \quad (9)$$

$$f = f_0 + (1 - f_0)\exp[-a(1 - a)] \quad (10)$$

Both expressions depend on the model parameters, a_0, p, f_0 and α that have to be adjusted. This approach offers more versatile capabilities than the use of a single law to capture the closure behaviour for a single joint. Indeed the classic way to proceed would be assumed that the mechanical aperture and the hydraulic aperture are equal and that the mechanical aperture varies in response to the normal stress changes can be captured by a simple non-linear and empiric law, as the hyperbolic one proposed by Bandis et al.(1983).

2.3.2 Open fracture

In this case, the main assumption is that the cubic law for flow in the fractures is valid in its incremental form. Any change in fracture aperture Δe results in a change in the hydraulic conductivity by a factor $(1 + \Delta e / e_0)^3$.

For a jacked-open cell i, the normal (e.g. z direction) discontinuity displacements φ_z^i produced by the mechanical stability analysis are turned into an increment of aperture for flow in the cell number i. From that follows the required expression for f at cell i:

$$f = \left(1 + \frac{\varphi_z^i}{e_o}\right)^3 \quad (11)$$

2.3.3 Sheared fracture

In each cell where some shearing develops, displacements in the local x and y directions are obtained, as φ_x^i and φ_y^i. A dilation angle δ is introduced to convert sliding into an irreversible contribution to the fracture aperture.

This effect is bounded to simulate fracture damages after some sliding occurs. We first built the cumulated displacement in the fracture plane, as $\xi = \xi_0 + d\xi$ with $d\xi = \sqrt{(\varphi_x^i + \varphi_y^i)}$ and ξ_0 the displacement obtained during the previous time step. Then the equivalent normal displacement is built according to

$$\Delta e = u \tan(\delta) \tanh\left(\frac{\xi}{u}\right) \quad (12)$$

The parameter u is insuring that the main part of the dilation takes place when the displacement ξ falls within [0, u]. A common magnitude for u is about 10 to 50 times e_0^i. Since some normal stress maintains contacts in a sheared situation, there is still the need to consider that the hydraulic conductivity depends on the ratio of contact area an as in the closed situation. Therefore both effects contribute to f and we assume

$$f = \{f_0 + (1 - f_0)\exp[-a(1 - a)]\}\left(1 + \frac{\Delta e}{e_0}\right) \quad (13)$$

2.3 Global hydraulic-mechanical model

In the transient fluid flow equation, a mass balance is established at each fracture cell and we assume that the rock is impervious and that

the fluid is compressible. Each portion of fracture is considered as an inflating or deflating single reservoir, that exchanges some fluid with the connected neighbouring cells. These local fluxes are built from the equivalent hydraulic conductivities of the bonds linking these adjacent elements and in proportion to the local head gradients. The hydraulic conductivity of a particular channel is built from a harmonic average of the hydraulic conductivities assigned to the two connected fracture elements. The local width of these channels is the length of the intersection segment of the adjacent cells.

Mass storage in a given disc is governed by the fluid compressibility, from the change of local aperture Δe, which results from the mechanical analysis, and from the change in contact area due to a unit change in effective stress. Classic prescribed hydraulic conditions can be applied at the model boundaries. These conditions apply at the elements of the mesh that intersect the geometrical surfaces used to define the hydraulic boundary. These conditions are of two types. The capabilities of the code include either the use of a constant head value or no flow at the outer surface of the model. Along the inner boundaries, namely along a borehole, sequences combining constant hydraulic heads or linearly variable hydraulic heads or a global flux can be applied. It is implicit that the element of the mesh forming the fracture edges within the rock mass are closed for flow.

The linear system of equations is solved for the hydraulic heads at each time step, but iterations are required due to the non-linear behaviour of the matrix coefficients. Hydraulic heads are turned into pressures and then used back again in the mechanical calculations in a two-step algorithm, until a prescribed tolerance on hydraulic head and discontinuity displacement is reached. To avoid cumbersome calculations in the mechanical part, the displacement discontinuities are solved upon a restricted sub-network made of cells that have the potential to shear or jack during the current time step. This subset of elements is updated at each time step and the corresponding influence matrix for the displacement discontinuity method is stored.

3. APPLICATION TO LE MAYET DE MONTAGNE FIELD DATA

3.1 Objective of the field study

The purpose of the field study performed by Cornet and Morin (1997) was to observe the gradual evolution of the hydrologic behavior of a fractured rock mass as a function of increasing pore pressure. The experiment was designed to measure the vertical distribution of hydraulic conductivity in a well by means of series of flow meter-injection tests, while progressively increasing the injected flow rate from the surface. The tested well, INAG III.9, is located at the Mayet de Montagne site (France) and was drilled nearly vertical in a granite horst. It extends down to 840 m. An inflatable packer was set at 275 m, and the injection takes place below, along the open hole section. As the pressure approached or exceeded the minimum principal stress magnitude in this section (Yin and Cornet, 1994), several new fluid-intake zones are emerged. Pressure could be maintained above this minimum value. These flow tests are summed up in Table 1.

3.2 Site description and construction of the fracture network

With the objective of simulating the global hydraulic behavior of a multiple fracture system, that exhibits different characteristics at different injection regime, we have to consider some

Table 1. Results of the flow logs at different injection rates, after Cornet and Morin (1997)

Global flow (l/min)	20	100	190	780
Pressure (MPa)	0.31	1.80	3.40	6.25
		Depth (m)		
>400	(-)	(-)	(-)	680
~450	(-)	(-)	75	130
~550	(-)	(-)	(-)	35
~640	8	32	45	45
< 750	12	68	70	70

(-) No contribution was noticeable

complexity in the geometry but also to keep it as simple as possible and close to reality, in order to allow tractable calculations and more conclusive discussions.

Five injected zones are identified along INAG III.9 borehole, as shown by flow meter logs (Table 1). Two of these zones, namely F3 and F4 in Table 2a, may correspond to fractured zones delineated in space with the help of induced micro-sismicity generated during earlier well tests, and discussed in Cornet and Scotti (1993). Strike, dip and extension for F3 and F4 are therefore constrained in the present model. The deepest zone, F5, is known to have good hydraulic properties since it was extensively developed during circulation tests in 1987 (Bruel and Cornet, 1995), but its orientation remains poorly documented. Both shallower zones, referred to F1 and F2 respectively, must be hydraulically active at a given flow regime while they remain non significant at lower regime. An output from Cornet and Morin (1997) experiments is that F2 contributes to the global injectivity as soon as injection over pressure reaches 3.4 MPa, while zone F1 controls the overall flow distribution when overpressure is about 6 MPa. Given the stress field determination from hydraulic tests on pre-existing fractures (see Fig. 3), the fracture F2 should be oriented in a direction nearly parallel to that of the principal maximum stress at the same depth. For similar reasons, F1 has to resist to fluid pressure

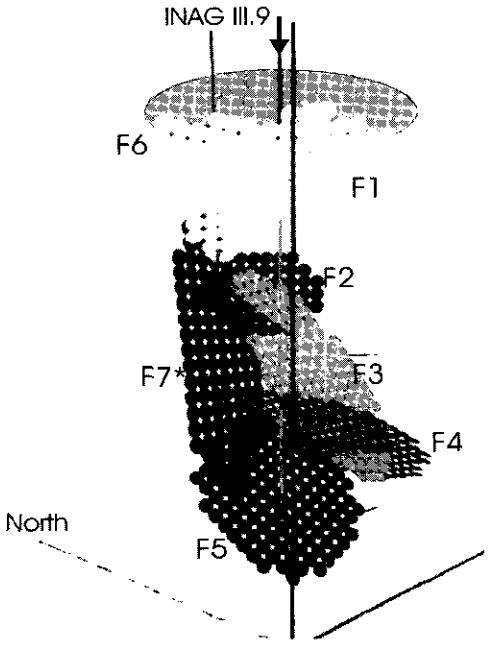

Fig. 2. Fracture assemblage, second alternative using F7*(see text), viewed from south-west. The cylindrical surface represents the external boundary of the model. The INAG III.9 borehole is the nearly vertical line close to the axis of the cylinder. The green circular area represents the hydraulic upper boundary and is situated 175 m below ground level

Table 2a. Selected fractures at the well INAG III.9

Name zone	Depth [m] / well head	Orientation [°] versus North	Extension Max. [m]
F1	-328.	N110 dip 45E	300
F2	-440.	N150 dip80W	200
F3	-502.	N184 dip61E	425
F4	-632.	N174 dip36E	300
F5	-770.	N110 dip60W	275

Table 2b. Selected fractures at the well INAG III.8

Name zone	Depth [m] / well head	Orientation [°] versus North	Extension Max. [m]
F6	-281	N110dip70E	300
F7	-472	N173dip83E	500
F7*	-484	N83dip83W	500

*Alternative orientation for structure F7, discussed in the text.

until a threshold larger than 3.6 MPa, is exceeded, thus implying it cannot be sub-parallel to F2.

Two other major conductive fatures are necessary to complete the fracture system. Both were observed in a nearby borehole, INAG III.8, drilled 100 m apart in the north-west direction. The main one, called here after F7, is sub-vertical, crosscut this second bore hole at a depth of 472 m below ground level and might have a large vertical extension, since this fracture has been found to be the host of natural flow prior to the drilling of the well. From a variety of geophysical loggings and hydraulic experiments, it was concluded that this fracture was sub parallel to the maximum horizontal stress at this depth. Imaging techniques suggest a North170 strike.

The last fracture referred to as F6, intersects the well INAG III.8 at about 317 m, with the orientation North 120 east and dipping 70 to the east. Hydraulic tests performed in 1984 during earlier experiment phases have shown it was able to support 6.5 MPa without mechanical reopening (Cornet et al. 1985). In the present investigation, F6 is supposed to link the fracture network with the shallower aquifers at the top of the system, while F7 will insure the global connectivity.

Other qualitative constraints are considered: we do not want a direct connection between F1 and the above hydraulic boundary, since we know from drilling that the upper part of the well INAG III.9 is poorly connected to these upper zones. We also assume that F2 is of limited extension, and this will be a key assumption for showing that a fracture can be jacked at a given pressure level, and meanwhile still able to support much higher pressure levels.

For simplicity we will assume that F1 and F6 are sub-parallel. Fracture sizes are calibrated so that F7 connects the six other fractures. Parameters used during the calculations are given in Table 2a and 2b. Fig. 2 illustrates this fracture assemblage.

Table 3. Stress regime at the well, expressed in MPa

Name zone	Depth [m] / well head	Normal stress	Shear stress	Effective* stress
F1	-328.0	8.69	1.34	5.47
F2	-440.0	7.75	0.95	3.42
F3	-502.0	10.55	2.50	5.63
F4	-632.0	14.90	2.95	8.71
F6	-281.0	7.97	1.60	5.21
F7	-472.0	8.45	1.47	3.83
F7*	-484.0	12.85	1.47	8.12

(*) Normal effective stress under hydrostatic conditions

3.3 Running the simulations

The simulated injection test proceeded in five steps. In the first and second steps, the water is injected at constant rates, respectively 20 l/min and 100 l/min. Each step is 6 hours long. The third phase is a shut in phase, 12 hours long. This causes the injected network to be depleted. Steps 4 and 5 are constant rate injection phases with 190 l/min during 7 hours and 780 l/min during 5 hours respectively. The hydraulic boundaries consist of a cylindrical surface, 200 m in radius, extending from 175 m below ground level down to 900 m depth, where a zero hydraulic head is prescribed. The horizontal top face of this volume is also assigned a zero hydraulic head boundary. The initial water pressure distribution corresponds to the hydrostatic equilibrium and initial normal and shear stresses prevailing at each fracture element (see Table 3) are derived from the in-situ stress tensor described in Fig. 3.

The results of the numerical simulations discussed here after concern the evolution of the injection pressure at the well head during time, as well as the evolution of the corresponding flow repartition at the different fractures along the open hole section.

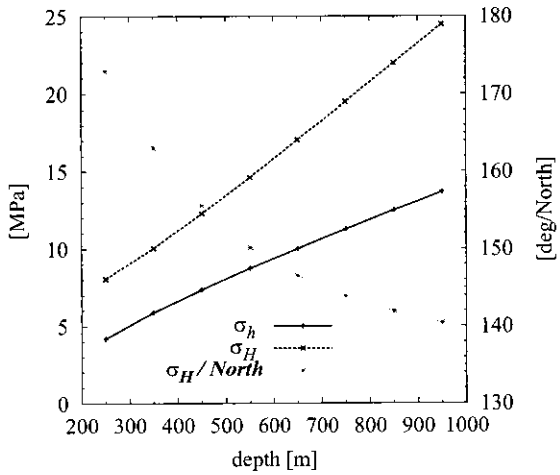

Fig. 3. Vertical evolution of the horizontal principal, maximum and minimum, stress components and orientation of the maximum horizontal stress versus north. (After Yin and Cornet, 1994). The vertical direction is assumed principal and vertical stress is given by the rock density

3.4 Results and discussion

3.4.1 First geometrical configuration

The numerical procedure, in a forward modeling sense, was run several times to find the most suitable configuration that matched the pressure transient data and the different flow logs. Although many sets of parameter may combine satisfactorily, we do not perform some systematic sensivity analysis and fracture apertures only were adjusted. Other parameters are kept fixed for all the calculations (Cf. Table 4).

As an initial configuration, we tested the hydraulic response of the fracture network made of the fractures F1 to F7 that were extracted from various geological and geophysical methods.

Phases one and two help us to define the hydraulic properties under low fluid pressure. Because most of the fluid has to be injected in the two deep zones, initial transmissivities at the top of the system have to be poor. We therefore get estimates for the parameters in equations (9) and (10) listed in Table 4.

During the fourth step, because the two deep zones support much higher normal stresses, injection pressure starts to increase and numerical results are more sensitive to the apertures of fractures F7 and F1, that are the natural paths for the fluid to exit the system. These aperture values were selected so that the threshold level of about 3.5 MPa level was reached within 5 hours of injection. According to this choice, fracture F2 becomes tensile, and fluid starts to be significantly injected there, as was observed on the field. At the end of this phase, the hydraulic head reaches 3.63 MPa and the calculated flow value in F2 rises up to 15.1 % of the total injected flow rate.

We now believe that assessing the validity of this model will be done by testing how the fifth phase can be predicted. An immediate output of this first attempt is that we failed to properly predict the last injection phase of the test using such a geometry, as illustrated in Fig. 4.

The main reason is that F7 is oriented nearly parallel to the maximum horizontal stress and therefore F7 and F6 form a preferential path for the fluid to escape upward as soon as F2 experiences some jacking.

Table 4. Model parameters used in the numerical simulations

Rock properties		
Young's modulus E	60000	MPa
Poisson's ratio ν	0.22	
Density	2.65	Kg m^{-3}
Fluid properties		
Dynamic viscosity	1. 10^{-3}	Kg $m^{-1}s^{-1}$
Density	1. 10^{3}	Kg m^{-3}
Fracture properties		
Separation law	a_0 = 0.50, p =7.5	
f-factor law	f_0=0.008, α=5.25	
friction coefficient	0.80	
Cohesion	0.0 (0.5)	MPa
dilation angle	2.	Deg.

Table 5. Calibrated apertures for the flowing zones

	Alternative 1 (F1+F2+ ... + F7)	
Fracture zone	e_0 [m]	Initial aperture [m]*
F1	0.000225	0.000128
F2	0.000150	0.000097
F3	0.000175	0.000098
F4	0.000460	0.000224
F5	0.000600	0.000295
F6	0.000200	0.000114
F7	0.000375	0.000186

(*) Equivalent value, at depth, under hydro-static condition, defined as $e = e_0 \times f^{1/3}$

Moreover F7 is subject to shear even earlier, already for fluid pressures as low as 2 MPa. This means that the downstream path to F2 becomes rapidly more and more attractive for fluid. Therefore, the fluid pressure increase during the fifth step is delayed and appears to be controlled by the shearing and dilation mechanism along the flow path F2 + F7 + F6. The pressure level of 6 MPa required to open the fracture F1 cannot be reached within the right time scale.

3.4.2 Second geometrical configuration

In order to stick with in-situ reality, we tested a second geometrical configuration by changing fracture F7 into a more resisting to shear fracture, hereinafter denoted F7*, and perpendicular to F7. (See parameters in Table 2b). We also increase the cohesion coefficient from 0 to 0.5 MPa, in order to get a more resistant network. Obviously this new geometrical model fails to reproduce the exact geometry at the borehole INAG III.8 but it offers the potential of different hydraulic behaviours. Indeed, it is possible to calibrate the aperture parameters against the first four phases, values are tabulated in Table 6, and let the model predict the last phase with much success. The results are described with Fig. 5. Fig. 6 compares at the end of both fourth injection steps, the spatial extension of the sheared and jacked zones within both geometric configurations.

Because F7* has the potential to resist to

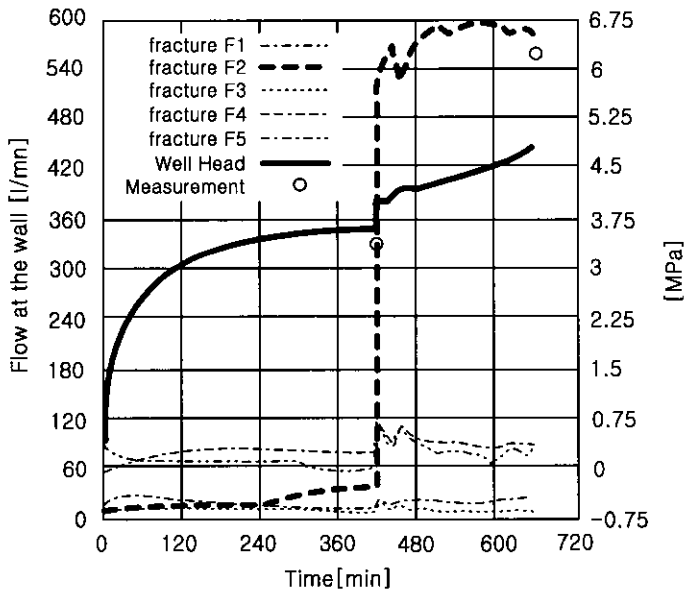

Fig. 4. Variation of injection pressure and flow rate during injection phases 4 and 5, at the various entry points for the first geometrical alternative

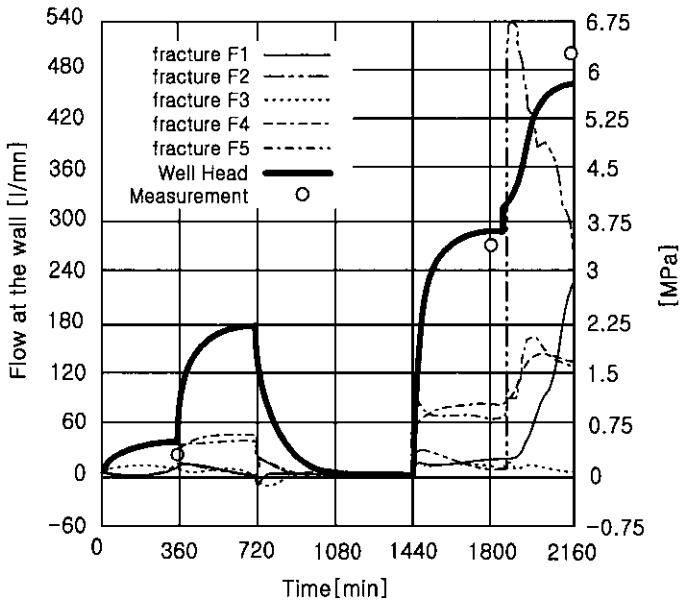

Fig. 5. Simulated injection head expressed in MPa, and flow distribution at F1, F2, ..., F5 entry points, versus time for the second geometrical configuration

higher effective normal stresses, the fracture F2 is now inflating (3.2×10^{-4} m at the end of step 4 and 4.1×10^{-3} m at the end of step 5) until an other flow path is activated to accommodate the large prescribed flow rate.

During a given time lap, fracture F1 and F2 are in competition, and flow is redistributed according to the current most attractive path. During the second half of phase 5, the pressure seems to stabilize although flow is progressively attracted by the fracture F1, at the top of the system (calculated aperture at the well of 4.7×10^{-4} m at the end of step 5). Thus the model shows that an increase of the aperture in fracture F2 can be simultaneously accompanied by a decrease in the accepted flow rate. In this case, and because we assume that stiff and poorly conductive structures exist that prevent tensile fractures to propagate, the driving hydraulic gradient through F2 in between the flowing boundaries (respectively, the bore hole and F7*) is decreasing and F2 tends to behave as a penny shape fracture with a uniform fluid pressure and little flow through it.

4. CONCLUSION

The results obtained from this in-situ experimental program are summarized in two ways. First, the collected data set demonstrates that

Table 6. Calibrated apertures for the second fracture network

	Alternative 1 (F1+F2+ ... + F7*)	
Fracture zone	e_0 [m]	Initial aperture [m]*
F1	0.000225	0.000128
F2	0.000150	0.000097
F3	0.000175	0.000098
F4	0.000460	0.000224
F5	0.000600	0.000295
F6	0.000225	0.000123
F7*	0.000400	0.000198

(*) Equivalent value, at depth, under hydro-static condition, defined as $e = e_0 \times f^{1/3}$

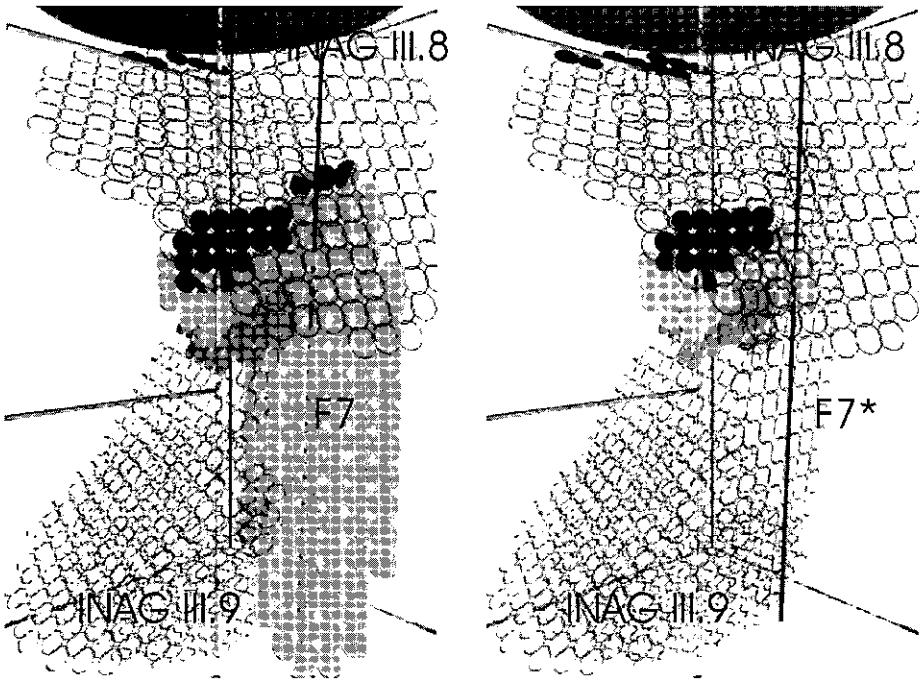

Fig. 6. Extension of the sheared area (light gray cells) and jacked area (dark gray cells) in the network for the geometrical first geometrical configuration (left) and second geometrical configuration (right)

fractures in natural systems can support fluid pressures larger than those one would have anticipated from the knowledge of the surrounding stress field. This may explain difficulties in any attempt of creating new fractures by hydraulic fracturing techniques at places where pre-existing discontinuities may insure the connectivity, even when they do not clearly participate to flow at moderated injection regimes. The discussion based on the two geometrical alternatives shows how a large structure close to an optimal orientation for frictional slip in the present day stress field can control the overall behavior at a large injection rate. A consequence from the above numerical experiment is that the global injectivity properties of a bore hole in a similar geological setting can not be extrapolated from the unique observation of the fractures intersecting it, otherwise the response in a pressure/flow diagram would in any case converge to the response of the single fracture, the most close to the jacking situation in that well.

Secondly, we point out that difficulties can be anticipated in the interpretation of pressure versus flow diagrams as soon as they are derived from injection tests performed upon fractures of unknown size. They should not be used to determine normal stresses to fractures without great caution, and without first establishing which process controls fluid pressure within such fractures. Transient analysis accounting for cumulated injected volumes should be preferred.

ACKOWLEDGEMENTS

The author would like to thank Prof. F.H. Cornet from IPG Paris for initiating this piece of work by sharing data and providing stimulating discussions. Code developments were supported

in related works by ADEME and the European Commission (DG XII), in the framework of renewable energy programs.

REFERENCES

Abdallah, G., Thoraval, A., Sfeir, A., and Piguet, J.P. (1995). "Thermal convection of fluid in fractured media." *Int. J. Rock Mech. Sci. & Abstr.*, Vol. 32, No.5, pp. 481-490.

Bandis, S. C., Lumsden, A. C., and Barton, N. R. (1983). "Fundamentals of rock joint deformation." *Int. J. Rock Mech. Sci. & Abstr.*, Vol. 20, No. 6, pp. 249-268

Brown, S. R. and Scholz, C. H. (1985). "Closure of random elastic surfaces in contact." *Journal of Geoph. Research*, **90**(B7), pp. 5531-5545

Bruel, D. and Cornet, F. H. (1995). "Forced fluid flow trough fractured reservoir s modelling." *In Fractured and Jointed rock Masses*, Edited by Myer, Cook, Goodman and Tsang, pp. 503-510.

Bruel, D. (1999). "Modelling hydraulic jacking tests on a pre-existing fracture system." *Proceedings Ninth International Congress on Rock Mechanics*, Rotterdam, Balkema, pp. 857-862.

Capasso, G., Scavia, C., Gentier, S., and Pellegrino, A. (1999). "The influence of normal load on the hydraulic behaviour of rock fractures." *Proceedings Ninth International Congress on Rock Mechanics*, Edited by Vouille and Berest, Rotterdam, Balkema, pp. 863-868.

Cornet, F. H., Bidaux, P., Binon, M., Blum, P. A., Couturie, J. P., Jolivet, J., Mosnier, J., Martel, L., Saleh, B., and Talebi, S. (1985). *Etude in situ de la percolation forcée d'eau en milieu fissure*. Résultats du programme Mayet de Montagne pour la période 1983-1985. Rapport AFME-INSU-PIRSEM, Institut de Physique du Globe de Paris.

Cornet, F. H. and Scotti, O. (1993). "Analysis of induced seismicity for fault zone identification." *Int. J. Rock Mech. Min. Sci. & Abstr.*, Vol. 30, No. 7, pp. 789-795.

Cornet, F. H. and Morin, R. H. (1997). "Evaluation of hydromechanical coupling in a granite rock mass from a high-volume, high-pressure injection experiment: le Mayet de Montagne, France". *Int. J. Rock Mech. & Min. Sci.* **34:3-4**, paper No. 207

Cundall, P. A. and Hart, R. D. (1985). *Development of generalized 2D and 3D Distinct Element Programs for modelling jointed rocks.* Misc. Paper SL-85-1, U.S. Army Corps of Engineers.

Gentier, S. (1986). *Morphologie et comportement hydroméchanique d'une fracture naturelle dans un granite sous contrainte normale : étude expérimental et téchnique,* Thèse de Doctorat, Univerité d'Oréans, 1986.

Jeong, W. C. (2000). *Modélisation de l'influence d'une zone de faille sur l'hydrogéologie d'un milieu fracture.* Thèse de l'Ecole Nationale supérieure des Mines de Paris, p. 278.

Pyrak-Nolte, L. (1992). "Interrelationships between the hydraulic and seismic properties of fractures." *Proceedinds. of ISRM International Conference on fractured and jointed rock masses,* Lake Tahoe, California, USA

Raven, K. G. and Gale, J. E. (1985). "Water flow in natural rock fracture as a function of stress and sample size." *Int. J. Rock Min. Sci. & Abstr.*, Vol. 22, pp. 251-261.

Rutqvist, J. (1995). "Determination of hydraulic normal stiffness of fractures in hard rock from well testing." *Int. J. Rock Min. Sci. &*

Abstr., Vol. 32, No. 5, pp. 513-523.

Sinha, K. P. (1979). *Displacement discontinuity technique for analysing stresses and displacements due to mining in seam deposit.* Ph.D. dissertation, University of Minnesota.

Stephansson, O., Jing, L. and Tsang, C. F. (editors) (1996). "Coupled Thermo-Hydromechanical processes of fractured media." Developments in geothechnical engineering (**79**), Elsevier, The Nederlands.

Unger, A. J. A. and Mase, C. W. (1993). "Numerical study of the hydromechanical behaviour of two rough fracture surfaces in contact." *Water Resources Research*, Vol.29, No.7, pp. 2101-2114.

Yin, J. M. and Cornet, F. H. (1994). "Integrated stress determination by joint inversion of hydraulic tests and focal mechanism." *Geoph. Res. Letters*, Vol. 21, No. 24, pp. 2645-2648.

Zimmerman, R. W. and Bodvarsson, G.S. (1996). "Hydraulic conductivity of rock fractures." *Transport in porous media*, No. 23, pp. 1-30.

Woo-Chang Jeong, Research Center for Disaster Prevention and Safety Management, Hong-Ik University, Seoul, Korea
(E-mail : jwc1967@hanmail.net)

Dominique Bruel, Centre d'Informatique Géologique, Ecole Nationale Superieure des Mines de Paris, Paris, France.

Jai-Woo Song, Department of Civil Engineering, Hong-Ik University, Seoul, Korea

(Received March 27, 2001 ; accepted June 18, 2001)